Publication

Biochimie 94 (2012) 1773–1783

Contents lists available at SciVerse ScienceDirect

Biochimie

journal homepage: www.elsevier.com/locate/biochi

Research paper

Dissecting substrate specificity of two rice BADH isoforms: Enzyme kinetics, docking and molecular dynamics simulation studies

Kultida Jiamsomboon [a], Witcha Treesuwan [c], Nonlawat Boonyalai [a,b,*]

[a] Department of Biochemistry, Faculty of Science, Kasetsart University, Chatuchak, Bangkok 10900, Thailand
[b] Center of Excellence for Innovation in Chemistry, Faculty of Science, Kasetsart University, Chatuchak, Bangkok 10900, Thailand
[c] Institute of Food Research and Product Development, Kasetsart University, Chatuchak, Bangkok 10900, Thailand

ARTICLE INFO

Article history:
Received 16 December 2011
Accepted 7 April 2012
Available online 16 April 2012

Keywords:
Betaine aldehyde dehydrogenase
Molecular docking analysis
Molecular dynamics simulation
Site-directed mutagenesis

ABSTRACT

Fragrance rice (*Oryza sativa*) contains two isoforms of BADH, named OsBADH1 and OsBADH2. OsBADH1 is implicated in acetaldehyde oxidation in rice plant peroxisomes, while the non-functional OsBADH2 is believed to be involved in the accumulation of 2-acetyl-1-pyrroline, the major compound of aroma in fragrance rice. In the present study, site-directed mutagenesis, molecular docking and molecular dynamics simulation studies were used to investigate the substrate specificity towards Bet-ald and GAB-ald. Consistent with our previous study, kinetics data indicated that the enzymes catalyze the oxidation of GAB-ald more efficiently than Bet-ald and the OsBADH1 W172F and OsBADH2 W170F mutants displayed a higher catalytic efficiency towards GAB-ald. Molecular docking analysis and molecular dynamics simulations for the first time provided models for aldehyde substrate-bound complexes of OsBADHs. The amino acid residues, E262, L263, C296 and W461 of OsBADH1 and E260, L261, C294 and W459 of OsBADH2 located within 5 Å of the OsBADH active site mainly interacted with GAB-ald forming strong hydrogen bonds in both OsBADH isoforms. Residues W163, N164, Q294, C296 and F397 of OsBADH1–Bet-ald and Y163, M167, W170, E260, S295 and C453 of OsBADH2–Bet-ald formed the main interaction sites while E260 showed an interaction energy of −14.21 kcal/mol. Unconserved A290 in OsBADH1 and W288 in OsBADH2 appeared to be important for substrate recognition similar to that observed in PsAMADHs. Overall, the results here help to explain how two homologous rice BADHs recognize the aldehyde substrate differently, a key property to their biological role.

1. Introduction

Aldehyde dehydrogenases (ALDHs) (E.C. 1.2.1.3) are a superfamily of NAD(P)$^+$-dependent enzymes which metabolize many biologically important intermediate aldehydes [1]. These aldehyde compounds are ubiquitous in nature and quite toxic to cells. Therefore, the regulation of the level of aldehyde intermediates must be carefully controlled. ALDHs catalyze the irreversible oxidation of aldehyde to their corresponding carboxylic acid. Some ALDHs can catalyze a very limited range of substrates whereas the others recognize a broad range of substrates. ALDH enzymes require either NAD$^+$ or NADP$^+$ as a cofactor [2] and the classification of ALDH members is determined by their aldehyde substrates such as alcohol, lactaldehyde and aminoaldehyde dehydrogenases. Aminoaldehyde dehydrogenases (AMADHs, EC 1.2.1.19) belong to the aldehyde dehydrogenase 9 family (ALDH9) [3] and are NAD(P)$^+$-dependent enzymes which can catalyze the oxidation of a broad range of ω-aminoaldehydes to the corresponding ω-amino acids. The ω-aminoaldehydes are obtained from the oxidation of polyamines such as spermine (Spm), spermidine (Spd) and putrescine (Put) which are oxidized by amine oxidases [4]. AMADH from *Pisum sativum* is an example of a plant AMADH that exhibits broad aminoaldehyde substrate specificity [5,6]. Besides AMADHs, plant betaine aldehyde dehydrogenases (BADHs, EC 1.2.1.8) also oxidize a wide range of ω-aminoaldehyde substrates in addition to its natural substrate, Bet-ald [8–10]. BADH enzymes generally catalyze the last step in the synthesis of the osmoprotectant glycine betaine from choline [11]. Thus, BADHs can be classified into two

Abbreviations: ALDH, Aldehyde dehydrogenase; AMADH, Aminoaldehyde dehydrogenase; 2AP, 2-acetyl-1-pyrroline; AP-ald, 3-aminopropionaldehyde; BADH, Betaine aldehyde dehydrogenase; Bet-ald, Betaine aldehyde; GAB-ald, γ-aminobutyraldehyde; IPTG, Isopropyl-β-D-thio-galactoside; MD, Molecular dynamics; TMAB-ald, 4-*N*-trimethylaminobutyraldehyde; TMAP-ald, 3-*N*-trimethylaminopropionaldehyde.

* Corresponding author. Department of Biochemistry, Faculty of Science, Kasetsart University, 50 Phahonyothin Road, Chatuchak, Bangkok 10900, Thailand. Tel.: +662 562 5555x2048; fax : +662 561 4627.
E-mail address: nonlawat.b@ku.ac.th (N. Boonyalai).

0300-9084/$ – see front matter © 2012 Elsevier Masson SAS. All rights reserved.
doi:10.1016/j.biochi.2012.04.009

subfamilies. The first group is those with high specificity for, and activity toward the substrate Bet-ald (true BADH) while the second group exhibits broad affinity for a range of aminoaldehydes (high BADH homology aminoaldehyde dehydrogenase (HBH-AMADH)) [7]. BADHs from rice have been previously shown to be an HBH-AMADH since they showed only moderate to low activity toward Bet-ald but high activity for aminoaldehydes [9,10,17]. Therefore, BADHs from rice can also be considered AMADHs [7].

At present, five crystal structures of BADHs and two crystal structures of plant AMADHs are available [6,12–14]. Most of the known structures of BADH are in tetrameric form, except for the plant AMADH which is dimeric. Each subunit of BADH comprises a coenzyme binding domain, an oligomerization domain and a catalytic domain. The catalytic triad of AMADH from *P. sativum* contains C294, N162 and E260 which are conserved in BADH from different species [6]. In the catalytic cycle of BADH, the catalytic cysteine attacks the aldehyde substrate forming a thiohemiacetal intermediate whereas the glutamate, which is involved in the proton relay system, has been proposed to be the general base in the catalysis. The asparagine on the other hand has been implicated in stabilizing the thiohemiacetal intermediate forming the oxyanion hole [14].

Two BADH homologs in rice (*Oryza sativa*), *OsBADH1* and *OsBADH2*, are encoded on chromosome four and chromosome eight, respectively [15] and share 75% amino acid sequence identity. It has been speculated that OsBADH1 is localized in rice plant peroxisomes [10] since its deduced primary structure contains a Ser–Lys–Leu (SKL) motif at the C-terminus, whereas an experiment in young panicles of rice plants used to identify the subcellular localization of OsBADH2 indicates that an OsBADH2 signal was only found in the cytoplasm and not in the nucleus [16]. Moreover, the eight base pair deletion in exon 7 of the *OsBADH2* gene results in a truncated non-functional OsBADH2 and the partial loss of OsBADH2 function is proposed to account for the accumulation of 2-acetyl-1-pyrroline (2AP), the major compound of aroma in fragrance rice [9,15]. Both OsBADHs have shown broad aminoaldehydes substrate specificity [9,10] and the enzymatic characterization of both OsBADHs showed that the enzymes can oxidize C3 and C4 aminoaldehydes or medium-chain aldehyde such as γ-aminobutyraldehyde (GAB-ald), 3-aminopropionaldehyde (AP-ald), 4-*N*-trimethylaminobutyraldehyde (TMAB-ald) and 3-*N*-trimethylaminopropionaldehyde (TMAP-ald) better than Bet-ald. Recently, it was reported that OsBADH2_Y420, containing a Y420 insertion similar to BADH2.8 from Myanmar fragrance rice, exhibited less catalytic efficiency towards GAB-ald but not for Bet-ald compared to the wild-type enzyme [17]. This mutant may bring about the accumulation of GAB-ald/Δ^1-pyrroline, which is subsequently converted to 2AP.

Although both OsBADHs are highly similar in amino acid sequence, their functions might be different. To elucidate and understand the substrate specificity of both OsBADHs, we first used site-directed mutagenesis of amino acids involved in catalysis and substrate recognition. Subsequently the cofactor NAD^+ binding to each enzyme was investigated to evaluate changes in enzyme conformation upon binding. The substrate specificity of the enzymes towards Bet-ald and GAB-ald was also investigated. In addition to biochemical experiments, molecular docking and molecular dynamics simulation were carried out to gain better understanding factors determining substrate specificity and catalysis.

2. Materials and methods

2.1. Materials

Betaine aldehyde chloride and γ-aminobutyraldehyde dimethyl acetal were obtained from Sigma–Aldrich Chemical Co. (St Louis, MO, USA) while acetaldehyde was purchased from Fluka A. G. (Buchs, Switzerland). Nicotinamide adenine dinucleotide (NAD^+) was obtained from Merck (Darmstadt, Germany). Ingredients for bacterial media and buffers were obtained from Himedia, USB and Acrōs Organic. Molecular biology reagents, including restriction enzymes, PCR reagents, DNA polymerase, DNA ladders and protein molecular weight standards, were obtained from Fermentas (USA). Hitrap Chelating HP columns were purchased from GE Healthcare Bio-Sciences AB (Uppsala, Sweden).

2.2. Bacterial strains and plasmids

Escherichia coli strains XL10-Gold (Stratagene, La Jolla, CA, USA) were used for cloning and isolation of plasmids. The pET28b-OsBADH1 and pET28b-OsBADH2 plasmids, containing the *OsBADH1* and *OsBADH2* genes, respectively, were constructed as described in Wongpanya et al. [17]. The *E. coli* strain BL21 (DE3) was used for protein expression.

2.3. Site-directed mutagenesis

OsBADH1 or OsBADH2 mutants were generated by PCR with the Quikchange® lightning site-directed mutagenesis kit from Stratagene (La Jolla, CA, USA), using the pET28b–OsBADH1 or pET28b–OsBADH2 plasmid [17] as a template, respectively. The mutagenic primers include mutations (underlined) at the corresponding triplets (bold) (only direct constructions are shown in Table 1). The presence of each specific mutation was confirmed by DNA sequencing.

2.4. Expression and purification of OsBADH wild-type and mutants

OsBADH1 and OsBADH2 enzymes, either wild-type or mutants, were produced in *E. coli* BL21 (DE3) using the pET28b expression system. Expression and purification of the enzymes were performed essentially as previously described with some modifications [17]. Transformed *E. coli* cells were taken from an LB-kanamycin plate and inoculated into 5 ml of LB-broth-kanamycin medium as overnight cultures. These starter cultures were subsequently used to inoculate 250 ml of LB-broth-kanamycin medium. The cultures were grown in a shaking incubator at 37 °C until A_{600} reached 0.4–0.6 and then protein expression was induced by adding IPTG to a final concentration of 0.4 mM. Induction progressed for 16–24 h at 22 °C before the cells were harvested by centrifugation (1900× *g* for 15 min) and stored at −20 °C.

The cell pellet was thawed and resuspended in 15 ml of extraction buffer (50 mM Tris–HCl pH 8, 0.5 mM NaCl and 5 mM imidazole). Cells were then broken by sonication using pulse amplitude (on 10 s, off 5 s) for 15 min. Cell debris was removed by centrifugation (11950× *g* for 30 min). The supernatant was filtered through a 0.45 μm pore diameter filter and then applied to a HiTrap Chelating HP column previously equilibrated with washing buffer A (50 mM Tris–HCl pH 8, 0.5 M NaCl and 0.03 M imidazole). Retained proteins were eluted with buffer B (50 mM Tris–HCl pH 8, 0.5 M

Table 1
Oligonucleotides used as primers for PCR site-directed mutagenesis.

Mutations	Mutagenic primer sequences (5′–3′)
N164A_OsBADH1	GGA CTT ATC ACT CCC TGG **GCT** TAT CCT CTG ATG GC
W172A_OsBADH1	TCT GCT GAT GGC TAC T**GC** GAA GGT TGC ACC TGC C
W172F_OsBADH1	CCT CTG CTG ATG GCT ACT **TTC** AAG GTT GCA CCT GC
N162A_OsBADH2	GGT TGA TCA CAC CTT GG**G** **CCT** ATC CTC TCC TGA TGG C
W170A_OsBADH2	TCT CCT GAT GGC AAC A**GC** GAA GGT AGC TCC TGC C
W170F_OsBADH2	CCT CTC CTG ATG GCA ACA **TTC** AAG GTA GCT CCT GC

NaCl and 0.5 M imidazole). Protein fractions were analyzed by 12% SDS-PAGE. Fractions containing purified enzyme were pooled and the buffer was exchanged with 50 mM HEPES-KOH, pH 8 to remove imidazole. Subsequently, the purified enzyme was stored at 4 °C for immediate use or −80 °C until future use.

2.5. Intrinsic fluorescence of OsBADH wild-type and mutants

Fluorescence measurements were carried out as described previously with some modifications [13]. Measurements were performed to investigate the binding of NAD^+ to OsBADH proteins. Fluorescence binding between proteins and NAD^+ was carried out by monitoring the intrinsic fluorescent intensity of tryptophan residues. Fluorescence titration was performed by adding microliter amounts of NAD^+ to 400 µl of 1.5 µM OsBADH in 50 mM HEPES-KOH buffer (pH 8). Excitation wavelength was 295 nm (slit 5 nm) and emission spectra were recorded between 300 nm and 450 nm (slit 5 nm). After addition of the cofactor, the sample was mixed and the spectrum was recorded. Titration results were corrected to account for ligand dilution in buffer. Data were plotted as ΔF_{max} (the maximum attainable change in fluorescence intensity) at 350 nm versus the concentration of cofactor. The dissociation constant (K_d) for NAD^+ was obtained by fitting the change in fluorescence against the concentration of NAD^+ using the following equation:

$$\%\Delta F_{obs} = \frac{\Delta F_{max}[L]_0}{K_d + [L]_0}$$

where $\%\Delta F_{obs}$ is the enhancement of fluorescence upon binding to protein, ΔF_{max} is the maximum attainable change in fluorescence intensity, $[L]_0$ is the total molar concentration of the ligand, and K_d is the dissociation constant for NAD^+ binding. The data were fitted and standard errors were calculated by non-linear regression analysis using the Microcal Origin 6.0 program.

2.6. Enzymatic activity of OsBADH wild-type and mutants

Enzyme kinetic assays for wild-type and mutant OsBADHs were measured spectrophotometrically by monitoring the oxidation of Bet-ald and GAB-ald [9]. Betaine aldehyde chloride was dissolved in H_2O and directly used in the enzymatic assay. γ-aminobutyraldehyde dimethyl acetal was used for GAB-ald. The diethylacetals of γ-aminobutyraldehyde were hydrolyzed with 1 M HCl and heated at 80 °C for 1 h. The hydrolyzate was neutralized by adding an equivalent volume of 1 N NaOH. Bet-ald and GAB-ald were stored at −20 °C while the 100 mM stock solution of acetaldehyde was prepared and kept at 4 °C until required. Enzymatic activities were determined using a reaction mixture containing 50 mM HEPES-KOH buffer, pH 8, 5 mM NAD^+ and various concentration of each substrate (between 8 and 1000 µM). One unit of enzyme activity was defined as the amount of enzyme that catalyzed the formation of 1 µmol of NADH per minute at 30 °C. Reactions was monitored by following the change in absorbance at 340 nm corresponding to the formation of NADH (ε = 6220 M^{-1} cm^{-1}) [9]. K_m and V_{max} values were obtained by fitting the initial rates against the concentration of each substrate to the Michaelis–Menten equation. The data were fitted and standard errors were calculated by non-linear regression using the Microcal Origin 6 software.

2.7. Molecular docking analysis

The crystal structure of OsBADH2 was obtained from Assist. Prof. Dr. Kiattawee Choowongkomon (Department of Biochemistry, Kasetsart University, Thailand) [18]. Since the amino acid sequence identity between OsBADH1 and OsBADH2 is about 75%, a homology model of OsBADH1 was generated by SWISS-MODEL using the crystal structure of OsBADH2 as a template. The structures of both OsBADH proteins were superimposed using the program PyMOL [19]. Bet-ald was taken from the crystal structure of *YdcW* (PDB entry 1WNB) [13] whereas GAB-ald was built using Discovery Studio 2.5 (Accelrys, Inc., CA, USA). Mutant proteins were generated using Discovery Studio 2.5. After both proteins and ligands were successfully constructed, the docking was performed on Autodock 4.0 [20]. For docking ligand, the rotational bonds of the side chain were treated as flexible whereas those of main chain were regarded as rigid. Grid boxes were created to cover the substrate-binding domain of the protein. The size of the grid box was set at 60 × 60 × 60 $Å^3$ and the center of the grid box was set at 7.545 Å (x), 3.238 Å (y), and 33.596 Å (z). The Lamarckian Genetic Algorithm (LGA) with 100 runs was used as the search algorithm. The population size was set at 150. Three-dimensional structures of OsBADHs–Bet-ald or OsBADHs–GAB-ald with the lowest energy and highest populations were visualized and analyzed by PyMOL [19] and Discovery Studio 2.5.

2.8. Molecular dynamics simulations

The selected models of OsBADHs–Bet-ald or OsBADHs–GAB-ald complexes obtained from docking were used for MD simulations. MD simulations were performed using the AMBER10 simulation package with the Cornell force field [21]. OsBADH1 and OsBADH2 contained 505 and 503 amino acid residues, respectively. All complexes were immersed in an octahedral box of TIP3P water [22] with the distance between solute surface and the edge of the box set at 10 Å. Minimization was achieved stepwise as follows: 2000 steps for hydrogen atoms, 2000 steps for solvent water molecules and 5000 steps for all atoms in the system. The equilibration was perfomed in the carononical ensemble (NVE) at 300 K; during the initial 100 ps all atoms in the protein were restrained while in the following 100 ps all atoms were set free. MD simulations were carried out under an isobaric–isothermal ensemble (NPT), at 1 atm and 300 K. Equilibration was achieved when the system was stable and this was followed by a production phase which was harvested during the last 500 ps of the trajectory. Root-mean-square displacement (RMSD) values for distances between interacting amino acid residues, hydrogen bonds and binding free energies were also calculated.

3. Results and discussion

3.1. NAD^+ cofactor binding

Several reports have previously shown that BADHs from several species can bind either NAD^+ or $NADP^+$ [6,8,13,17]. BADHs from rice, OsBADH1 and OsBADH2, have greater affinity for NAD^+ than for $NADP^+$ [17]. The affinity of each enzyme for NAD^+ was investigated by monitoring changes in intrinsic tryptophan fluorescence upon binding. For BADHs, it has been reported that the binding of NAD^+ usually takes place prior to the binding of aldehyde substrate [23]. When the wavelength at 295 nm was used to excite the tryptophan residues within the protein, the emission spectrum of OsBADHs exhibited maxima at 350 nm. A decrease in the intensity of tryptophan fluorescence for OsBADHs was observed upon the addition of NAD^+. This phenomenon was clearly associated with the binding of NAD^+ implying that the overall structure of the enzyme was correct and that mutations to the OsBADH active site do not induce significant changes in conformation. Dissociation constant (K_d) values for OsBADH1 and OsBADH2 wild-type and mutants were determined for NAD^+ and are shown in Table 2. K_d

Table 2
Dissociation constant (K_d) of NAD^+ and OsBADHs.

K_d (μM)			
OsBADH1		OsBADH2	
Wild-type	34 ± 3	Wild-type	9 ± 1
N164A	51 ± 3	N162A	19 ± 4
W172A	56 ± 3	W170A	16 ± 3
W172F	50 ± 3	W170F	14 ± 2

values of all mutants increased by less than 2-fold, indicating that each mutation mentioned herein did not dramatically affect protein structure or cofactor binding. The K_d values reported here were in agreement with a previous study [17]. However, the K_d value of OsBADH2 for NAD^+ (9 μM) suggested that OsBADH2 can bind to NAD^+ with higher affinity compared to OsBADH1 (K_d of 34 μM). Collectively, the results showed that each mutant could bind NAD^+, indicating they are correctly folded. Having determined the cofactor binding affinity, the kinetic parameters K_m, k_{cat} and k_{cat}/K_m for OsBADH wild-type and mutants were also characterized using Bet-ald and GAB-ald as substrates.

3.2. Enzymatic characterization

All OsBADH1 and OsBADH2 wild-type and mutants can catalyze the oxidation of Bet-ald and GAB-ald as shown in Table 3. The K_m value of wild-type OsBADH1 for Bet-ald was 3-fold higher than GAB-ald, suggesting that OsBADH1 can bind GAB-ald with a higher affinity than Bet-ald. The K_m values for the OsBADH1 mutants were about 7–10-fold lower than that of the wild-type OsBADH1, respectively, while K_m values for the OsBADH1 mutants for GAB-ald were 1.5–6.6-fold lower. These results showed that all OsBADH1 mutants seemed to bind both Bet-ald and GAB-ald tighter than wild-type OsBADH1. Similar to OsBADH1, the K_m value of wild-type OsBADH2 for Bet-ald was 6.6-fold higher than GAB-ald while the K_m values of the OsBADH2 mutants for Bet-ald were observed to have a 3.3–4.4-fold lower, respectively compared to wild-type OsBADH2. In contrast, K_m values of the OsBADH2 mutants for GAB-ald showed a 1.5–2.8-fold increase, respectively compared to wild-type OsBADH2. These results indicated that mutants of OsBADH2 could bind Bet-ald tighter than wild-type but bind GAB-ald slightly less than wild-type. When comparing the K_m values of OsBADH1 and OsBADH2 for Bet-ald and GAB-ald to those previously reported [9,10,17], our results are comparable in that the enzymes can bind GAB-ald better than Bet-ald.

For catalytic activity, the k_{cat} values of the OsBADH1 mutants for Bet-ald were found to be between 16 and 236-fold lower, respectively, while those of the OsBADH1 mutants for GAB-ald were around 1.4–13.5-fold lower, respectively, compared to wild-type OsBADH1. For the OsBADH2 mutants, the k_{cat} values for Bet-ald were 3.8–8-fold lower compared to wild-type OsBADH2. Likewise, the k_{cat} values of N162A and W170A for GAB-ald were 2.7-fold and 3.2-fold lower compared to the wild-type, respectively, but the W170F mutant had k_{cat} values 4.4-fold larger compared to that of the wild-type. Collectively, the results revealed that substitution of N164 and W172 of OsBADH1 and N162 and W170 of OsBADH2 by alanine reduced the catalytic activity towards Bet-ald and GAB-ald. However, the OsBADH2 W170F mutant exhibited a slightly higher k_{cat} value than the wild-type while OsBADH1 W172F exhibited a reduced k_{cat} value. For the catalytic efficiency, the k_{cat}/K_m values of the OsBADH1 mutants for Bet-ald were reduced by 2.1–23.8-fold, while the k_{cat}/K_m value of N164A for GAB-ald were 2.4-fold lower but the k_{cat}/K_m values of W172A and W172F for GAB-ald were unchanged and 2-fold higher, respectively compared to OsBADH1 wild-type. For OsBADH2 mutants, the k_{cat}/K_m values of N162A and W170A for Bet-ald were 1.6-fold and 2.4-fold lower, respectively but the k_{cat}/K_m value of W170F for Bet-ald was 1.2-fold higher. Similarly, the k_{cat}/K_m values of N162A and W170A for GAB-ald were 7.5-fold and 4.9-fold lower, respectively while the k_{cat}/K_m value of W170F for GAB-ald was 1.6-fold higher. Out of six mutants, only two mutants (OsBADH1 W172F and OsBADH2 W170F) showed a higher catalytic efficiency towards GAB-ald. This implied that either W172 or W170 in each protein may be key residues determining substrate specificity towards GAB-ald. In addition to Bet-ald and GAB-ald, acetaldehyde was also used as a substrate since it was previously reported that both OsBADH1 and OsBADH2 catalyzed the oxidation of acetaldehyde [10]. Our results (Table 4) were in agreement with those previously reported indicating that OsBADH1 is a better candidate enzyme for acetaldehyde than OsBADH2.

Table 4
Kinetic parameters for wild-type OsBADHs with acetaldehyde.

Acetaldehyde			
	K_m (μM)	k_{cat} (s^{-1})	k_{cat}/K_m (M^{-1} s^{-1})
OsBADH1	99 ± 29	0.14	1425
OsBADH2	146 ± 34	0.08	607

BADH enzyme from *E. coli* was reported to be able to catalyze the oxidation of GAB-ald better than Bet-ald in general because of the shape of its active site [13]. Mutagenesis of the highly conserved N162 of PsAMADH2 to alanine resulted in about a 200-fold reduction in dehydrogenase activity, indicating that the residue is involved in the catalytic efficiency of PsAMADH2 [6]. Therefore, mutation of the catalytic Asn residue would definitely affect the k_{cat}/K_m value. Besides the catalytic triad, Trp residues lining the substrate binding pocket were proposed to be involved in substrate binding [12], and hence mutation of these Trp residues should also affect k_{cat}/K_m. Most of the mutants examined herein exhibited lower or equal catalytic efficiency towards Bet-ald, while some mutants showed an increased catalytic efficiency towards GAB-ald compared to the wild type. Additionally, changing Trp to Phe had a tremendous effect on k_{cat}/K_m towards GAB-ald but not towards Bet-ald indicating that Trp may be involved in the recognition of Bet-ald but not GAB-ald. Our result correlated well with a previous

Table 3
Kinetic parameters for wild type and mutant OsBADHs with Bet-ald and GAB-ald.

	OsBADH1							OsBADH2					
	Bet-ald			GAB-ald				Bet-ald			GAB-ald		
	K_m (μM)	k_{cat} (s^{-1})	k_{cat}/K_m (M^{-1} s^{-1})	K_m (μM)	k_{cat} (s^{-1})	k_{cat}/K_m (M^{-1} s^{-1})		K_m (μM)	k_{cat} (s^{-1})	k_{cat}/K_m (M^{-1} s^{-1})	K_m (μM)	k_{cat} (s^{-1})	k_{cat}/K_m (M^{-1} s^{-1})
Wild-type	1288 ± 192	0.52	405	432 ± 57	0.31	718	Wild-type	251 ± 62	0.057	228	38 ± 11	0.032	842
N164A	165 ± 35	0.032	194	78 ± 5	0.023	295	N162A	66 ± 10	0.0093	141	107 ± 12	0.012	112
W172A	129 ± 23	0.0022	17	291 ± 18	0.22	756	W170A	77 ± 7	0.0072	94	58 ± 8	0.01	172
W172F	140 ± 51	0.0102	73	65 ± 11	0.09	1385	W170F	57 ± 10	0.015	263	105 ± 10	0.14	1333

study of aromatic active-site residues in PsAMADH2 [24] which showed that W170, W288 and Y163 (PsAMADH2 numbering), were important for the overall geometry of the substrate channel allowing for the appropriate orientation of the substrate towards the catalytic residue C294. These residues are also essential for π-electron stacking interaction with an entering substrate. Alanine scanning of aromatic residues in the substrate channel resulted in a change in the substrate specificity of PsAMADH2 [24]. Since no crystal structures of enzyme/aldehyde complexes or of OsBADH are currently available, we used molecular docking and molecular dynamics simulation to gain a better understanding of factors determining differences in substrate specificity.

3.3. Molecular docking analysis

The crystal structure of OsBADH2 [18] was used as a template to generate a homology model of OsBADH1 (residues 8–504) using SWISS-MODEL. The quality of the OsBADH1 model was evaluated using the program PROCHECK [25]. The model possessed good geometry, with 85% of all residues in the most favored and 14.6% in the allowed regions of the Ramachandran plot (Supplementary data Fig. S1). The RMSD value between OsBADH1 and PsAMADH2 was 0.57 Å. To confirm the reliability of the results from molecular docking, the structure of OsBADH-substrate complexes from docking were superimposed with the structure of PsAMADH1 (PDB

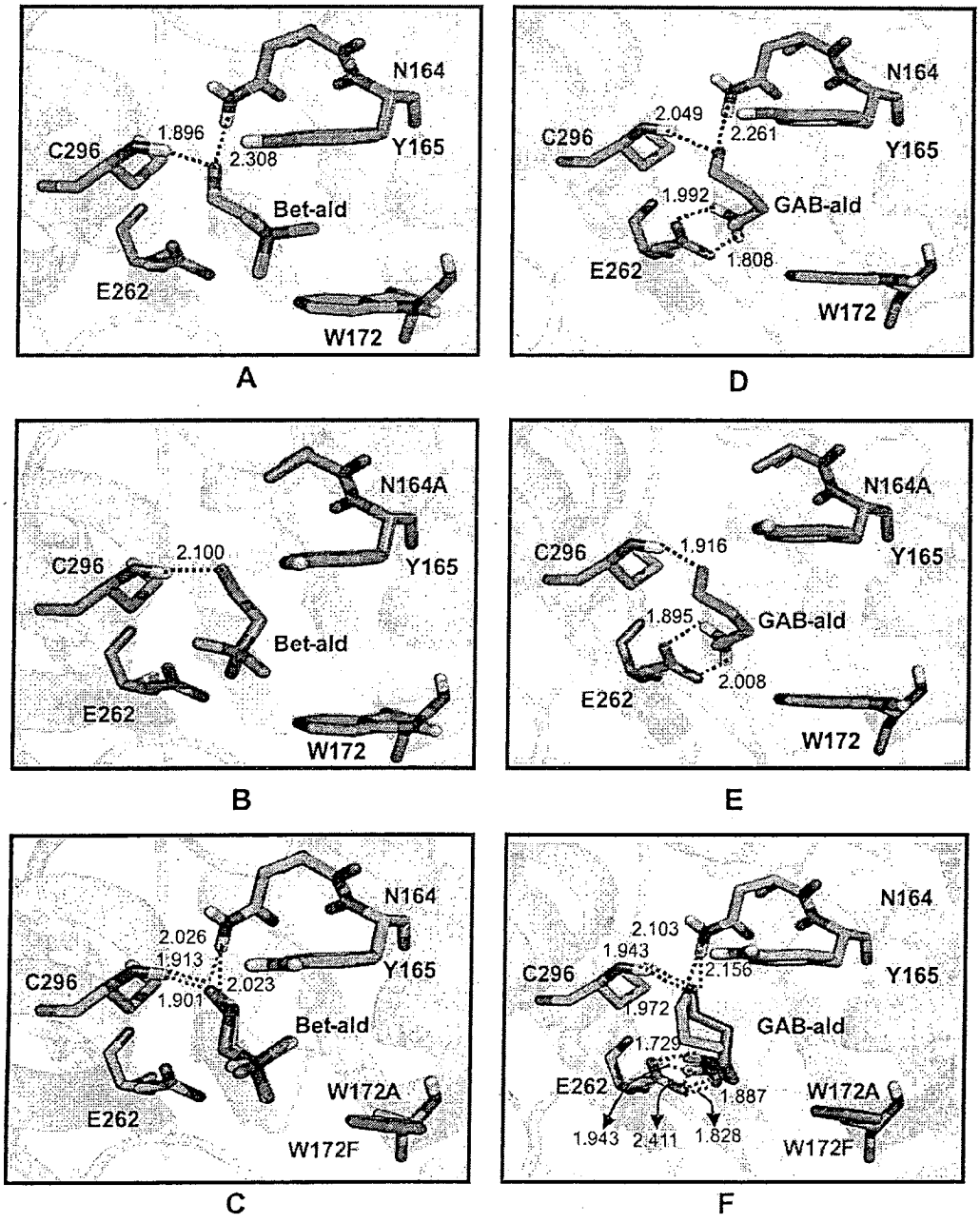

Fig. 1. Molecular docking analysis of (A) OsBADH1 with Bet-ald (B) N164A with Bet-ald (C) W172A and W172F with Bet-ald (D) OsBADH1 with GAB-ald (E) N164A with GAB-ald and (F) W172A and W172F with GAB-ald. Hydrogen bonds are shown as dotted lines. Carbon atoms of OsBADH1, N164A, W172A and W172F are colored in green, orange, cyan and magenta, respectively. The names of catalytic triad residues for OsBADH1 including C296, E262 and N164 are colored in red while the aldehyde substrates, Bet-ald and GAB-ald are in green. Distances are in angstrom. (For interpretation of the references to color in this figure legend, the reader is referred to the web version of this article.)

entry 3IWK) [6] using PyMOL [19]. The position of both Bet-ald and GAB-ald overlapped well with the glycerol molecule in PsAMADH1 (Supplementary data Fig. S2). For the OsBADH-substrate complexes GAB-ald displayed a lower binding energy than Bet-ald, indicating that GAB-ald is likely to bind both OsBADH1 and OsBADH2 with high affinity (Supplementary data Table S1). The binding pockets of OsBADH1 and OsBADH2 in complex with Bet-ald and GAB-ald are shown in Figs. 1 and 2 with the hydrogen bonding analysis. It can be seen that the carbonyl group of Bet-ald can form two moderate to strong hydrogen bonds between the N–H main chain of C296 and the N–H side chain of N164 in the OsBADH1–Bet-ald complex (Fig. 1A). In the N164A–OsBADH1-Bet-ald complex, the hydrogen bond between the N–H side chain of N164 and the carbonyl group of Bet-ald was abolished when residue N164 was replaced with alanine (Fig. 1B). In the W172A- and W172F–OsBADH1-Bet-ald complexes, two strong hydrogen bonds were also observed similar to those in wild-type OsBADH1 (Fig. 1C). However, the hydrogen bond distances in all mutants were slightly longer than those observed in the wild-type enzyme. It is important to note that the tertiary amine group of Bet-ald was positioned away from the mutated residue whereas the oxygen was positioned toward the catalytic cysteine. Unlike the OsBADH1–Bet-ald complex, four hydrogen bonds were observed in wild-type OsBADH1–GAB-ald and W172A–OsBADH1-GAB-ald while five hydrogen bonds are

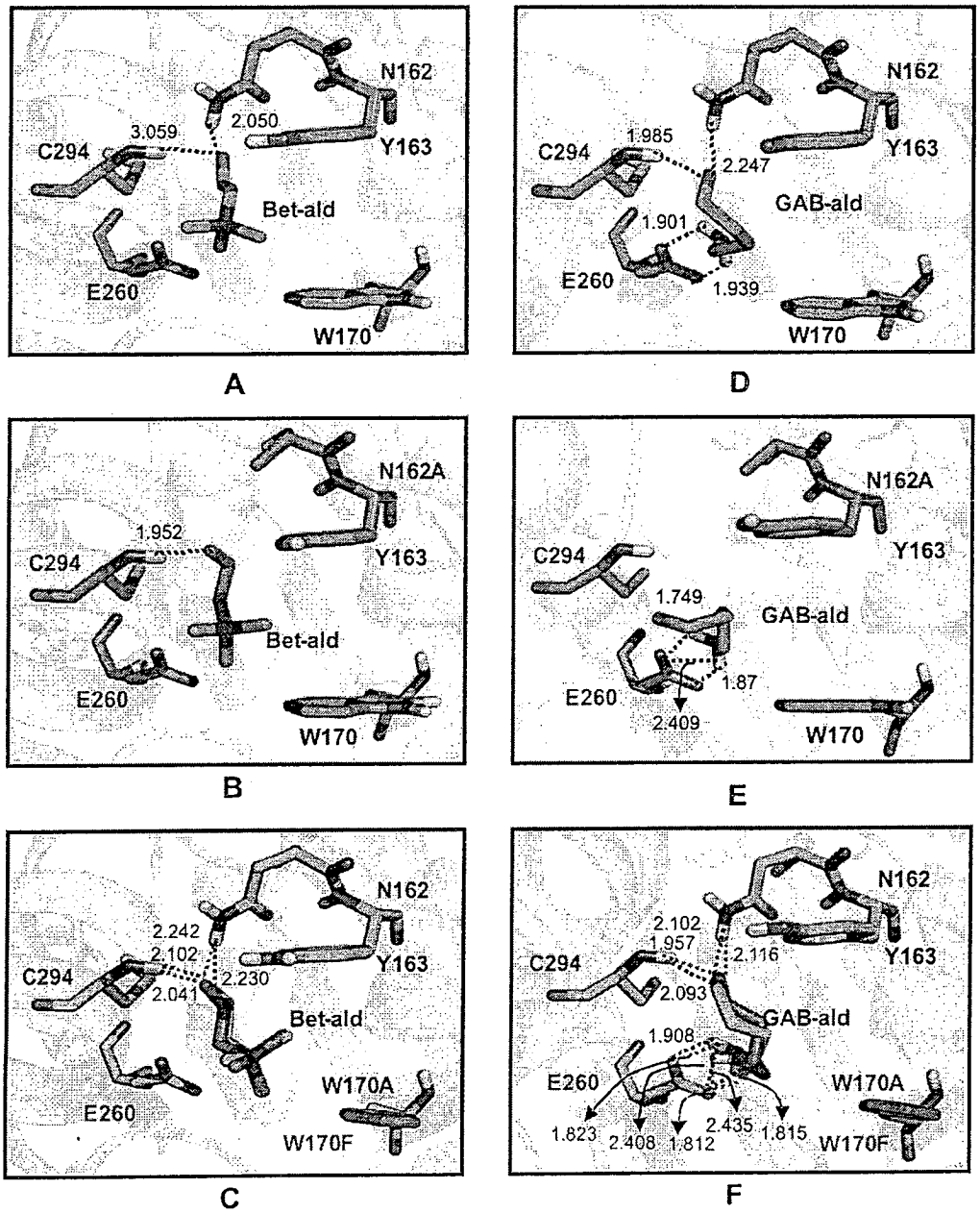

Fig. 2. Molecular docking analysis of (A) OsBADH2 with Bet-ald (B) N162A with Bet-ald (C) W170A and W170F with Bet-ald (D) OsBADH2 with GAB-ald (E) N162A with GAB-ald and (F) W170A and W170F with GAB-ald. Hydrogen bonds are shown as dotted lines. Carbon atoms of OsBADH2, N162A, W170A and W170F are colored in green, orange, cyan and magenta, respectively. The names of the catalytic triad residues for OsBADH2 including C294, E260 and N162 are highlighted with red text. Bet-ald and GAB-ald are designated by green text. Distances are in angstrom. (For interpretation of the references to color in this figure legend, the reader is referred to the web version of this article.)

observed in W172F–OsBADH1-GAB-ald (Fig. 1F). In the OsBADH1 mutant – GAB-ald complexes, the hydrogen bond between the N–H side chain of N164 and the carbonyl group of GAB-ald was also disturbed when residue N164 was changed to alanine (Fig. 1E). Higher numbers of hydrogen bonds in the GAB-ald complex correlate well with the kinetic results in which K_m values for GAB-ald were slightly lower than those for Bet-ald. It was also noted that the amino group in GAB-ald was pointed toward E262 instead of W172. These results offer a possible explanation for the observed differences in substrate specificity for OsBADH1.

In comparison to the OsBADH1–Bet-ald complex, similar hydrogen bonding networks were observed in the OsBADH2–Bet-ald complex. The N–H main chain of C294 and the N–H side chain of N162 could form hydrogen bonds with the oxygen atom of the carbonyl group of Bet-ald as seen in the OsBADH1 complex (Fig. 2A). Similar to OsBADH1, the N162A mutation resulted in the loss of a hydrogen bond (Fig. 2B) but the same pattern of hydrogen bonds is observed in the W170A and W170F complexes (Fig. 2C). For the OsBADH2–GAB-ald complex, four hydrogen bonds can be found between GAB-ald and residues C294, N162 and E260 (Fig. 2D). It is noteworthy that two hydrogen bonds between N–H of GAB-ald and the carboxyl group of E260 are only detected in the complex with GAB-ald. However, in the N162A–GAB-ald complex, only hydrogen bonds between the side chain of E260 and Bet-ald are observed (Fig. 2E). On the other hand, five hydrogen bonds are observed in both the W170A–GAB-ald and W170F–GAB-ald complexes (Fig. 2F). To further examine the binding mode of both Bet-ald and GAB-ald to wild-type OsBADHs as well as to determine interactions involved in the protein–ligand complex, four complexes of the wild-type enzymes (OsBADH1–Bet-ald, OsBADH1–GAB-ald, OsBADH2–Bet-ald and OsBADH2–GAB-ald) obtained from the docking experiment were used for MD simulations.

3.4. MD simulations and binding energy of OsBADH complexes

Structural and dynamic studies of both OsBADHs with aldehyde substrates were carried out by MD simulations. The OsBADH complex comprised OsBADHs, NAD^+, and their aldehyde sub strates. The trajectories for four simulation systems: OsBADH1–Bet-NAD^+, OsBADH1–GAB-NAD^+, OsBADH2–Bet-NAD^+ and OsBADH2–GAB-NAD^+, were analyzed over the last 500 ps after reaching equilibrium. RMSD fluctuations for OsBADH complexes were monitored to determine the structural equilibrium (Supplementary data Fig. S3). Overall, the results confirmed that all components were well in equilibration throughout the analysis range thus allowing us to determine binding energies and preferred binding sites for each complex.

Thermodynamic parameters for OsBADHs–Bet-ald and OsBADHs–GAB-ald complexes are presented in Table 5. The energy component involved in binding indicated that the simulation models could be separated into two sets based on the ligand driving force for the interaction. Set I was the binding of OsBADHs to Bet-ald. The important interactions for these models were electrostatic interactions (ΔE_{ELE}), which played a major role as the main attractive force. The *van der Waal* interactions in the gas phase (ΔE_{VDW}) were the second most important energy component for this binding. Set II contained models of OsBADHs binding to GAB-ald in which, unlike OsBADHs–Bet-ald, the electrostatic interaction was not the main interaction. Electrostatic interactions for OsBADH1 and OsBADH2 were −22.62 and −22.67 kcal/mol, respectively, while the *van der Waal* interaction was −17.74 kcal/mol for OsBADH1 and −19.05 kcal/mol for OsBADH2. It is noted that the nonpolar interaction of solvation ($\Delta\Delta G_{SA}$) of the four complexes was lower than the *van der Waal* interaction in gas phase

Table 5
Binding free energies for four trajectories of the OsBADH1–Bet-ald, OsBADH1–GAB-ald, OsBADH2–Bet-ald and OsBADH2–GAB-ald complexes.

Energy (kcal/mol)	OsBADH1		OsBADH2	
	Bet-ald	GAB-ald	Bet-ald	GAB-ald
ΔE_{ELE}[a]	−239.51	−22.62	−224.06	−22.67
ΔE_{VDW}[b]	−20.53	−17.74	−17.82	−19.05
$\Delta\Delta G_{SA}$[c]	−2.85	−2.65	−2.85	−2.70
$\Delta\Delta G_{PB}$[d]	246.01	24.66	227.09	28.64
$\Delta\Delta G_{MM/PBSA}$[e]	−16.88	−18.34	−17.65	−15.78

[a] Electrostatic energy.
[b] van der Waals energy.
[c] Nonpolar contribution to solvation.
[d] Electrostatic contribution to solvation.
[e] Total binding energy.

(ΔE_{VDW}). This may be caused by hydrogen bonding interactions during complex formation, resulting in the reduction of the polar surface exposed to water solvent. Additionally, the unfavorable energy component might have resulted from the electrostatic contributions of solvation ($\Delta\Delta G_{PB}$), which are 246.01, 24.66, 227.09 and 28.64 kcal/mol for OsBADH1–Bet-ald, OsBADH1–GAB-ald, OsBADH2–Bet-ald and OsBADH2–GAB-ald, respectively. According to the total binding energy of OsBADH1–ligand complexes, GAB-ald was represented as a higher potential ligand for OsBADH1 than Bet-ald with $\Delta\Delta G_{MM/PBSA}$ of −18.34 kcal/mol, which agreed well with the kinetic result. However, in contrast to the kinetic data the binding energy of OsBADH2–Bet-ald (−17.65 kcal/mol) was stronger than OsBADH2–GAB-ald (−15.78 kcal/mol). To confirm our results, the simulation experiments were carried out in triplicate and the similar results were obtained. While the binding energy from docking in which the conformation of the enzyme was kept rigid correlated well with the kinetic results, MD simulations in which the enzyme and ligands were allowed to be flexible revealed a slightly different binding energy. This suggested that the dynamics of OsBADHs and the aldehyde substrates significantly affected the binding event. Conformational changes of amino acid residues around the binding site of OsBADH2 are discussed in the next section.

Unlike molecular docking, MD simulations allowed the protein–ligand complex to be fully relaxed in the solvent environment, thereby generating more reliable binding properties. In the OsBADH1 system, the OsBADH1–GAB-ald complex showed the lowest binding energy from docking and exhibited the best binding from molecular dynamics simulation. However, in the OsBADH2 system, the OsBADH2–GAB-ald complex gave the lowest binding energy from docking but not from MD simulations. In order to understand this difference, hydrogen bonding interactions and MMGBSA decomposition of the binding energy were considered.

3.5. Protein–ligand interactions

A statistical analysis of the equilibrium distance and hydrogen bonding interactions during the course of the MD simulation revealed that some atoms of the ligands and the enzyme moved closer to or further from each other due to the dynamics in the binding process. The conformation of either Bet-ald or GAB-ald upon binding to both OsBADH complexes was examined as shown in Fig. 3. In OsBADH1–Bet-ald, only one hydrogen bond was observed (Fig. 3A) between the main chain of C296 (N) and the oxygen atom (O) of Bet-ald. In OsBADH1–GAB-ald, the four observed hydrogen bonds were between (Fig. 3B): E262 (O) and GAB-ald (H1), GAB-ald (N1) and W454 (HE1), GAB-ald (O1) and C296 (H) and L263 (O) and GAB-ald (H2). In OsBADH2, no hydrogen bonds were observed for Bet-ald (Fig. 3C) but five hydrogen bonds

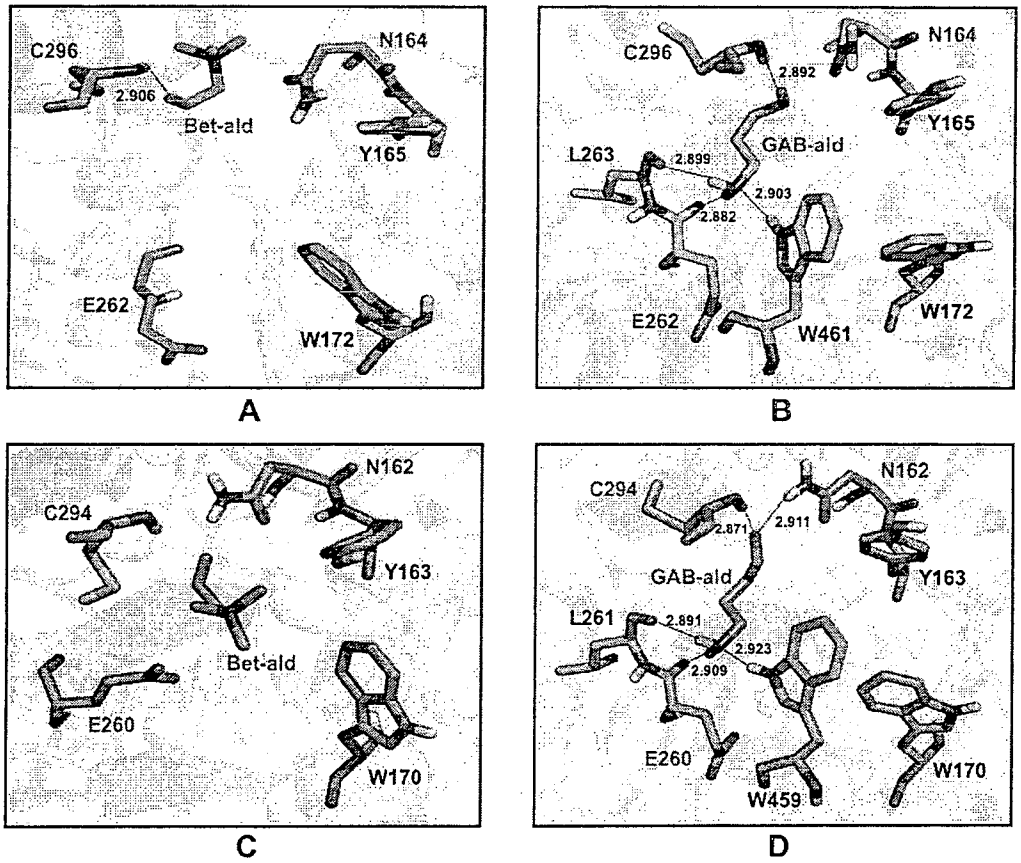

Fig. 3. MD simulations of the active site of (A) modeled OsBADH1 with Bet-ald (B) OsBADH1 with GAB-ald (C) OsBADH2 with Bet-ald and (D) OsBADH2 with GAB-ald. Hydrogen bonds are shown as dotted lines. Carbon atoms of OsBADH1–Bet-ald, OsBADH1–GAB-ald, OsBADH2–Bet-ald and OsBADH2–GAB-ald are colored in green, cyan, orange and magenta, respectively. The names of catalytic triad residues for OsBADH1 including C296, E262 and N164 and OsBADH2 including C294, E260 and N162 are colored in red. Bet-ald and GAB-ald are designated with pink text. Distances are in angstrom. (For interpretation of the references to color in this figure legend, the reader is referred to the web version of this article.)

were observed for GAB-ald (Fig. 3D). The five hydrogen bonds in the OsBADH2–GAB-ald complex were between GAB-ald (O1) and C294 (H), L261 (O) and GAB-ald (H2), GAB-ald (O1) and N162 (HD21), GAB-ald (N1) and W456 (HE1) and E260 (O) and GAB-ald (H1).

In the light of the MD simulations, it was revealed that GAB-ald formed stronger hydrogen bonds than Bet-ald with OsBADH1. As for OsBADH2, five hydrogen bonds were formed in the OsBADH2–GAB-ald complex while none was observed in OsBADH2–Bet-ald complex. In addition to hydrogen bond formation, relationships between the orientation of the Bet-ald and GAB-ald in the complex were different. First, Bet-ald in the OsBADH1 complex was far away from the catalytic triad compared with that in the OsBADH2 complex. It is important to note that the position of Bet-ald observed in the crystal structure of BADH in *E. coli* was also different from that in PaBADH [13]. Secondly, when looking at the two substrates, GAB-ald was located closer to the catalytic residue, E262, compared to Bet-ald. This finding was in agreement with a previous work, which reported that BADH catalyzes the oxidation of GAB-ald (C3–C6 aminoaldehydes) better than Bet-ald [5,6,10].

3.6. Energy decomposition of the binding energy

To gain more details in the energy of binding, interactions between ligand and surrounding residues within 5 Å were observed through decomposition energy using the MMGBSA (Molecular Mechanics-Generalized Born Surface Area) method as implemented in AMBER10. Eighteen residues within 5 Å radius of each OsBADH active site interacting with the substrate aldehydes were observed (Supplementary data Table S2) and the interaction energies were shown in Supplementary data Table S3. Alignment of the amino acid sequences for the OsBADHs showed that most residues are identical (Supplementary data Fig. S4) except for the two following residues: residue 290 (Ala in OsBADH1 and Trp in OsBADH2) and residue 295 (Val in OsBADH1 and Ile in OsBADH2). It is interesting to note that a change from aliphatic to aromatic amino acids was seen at position 290 while at position 295 a change is conservative (Val to Ile). Interactions between ligand and a selection of eighteen different residues were calculated as shown in Fig. 4A and B. It can be seen that three residues (W163, N164 and C296) mainly interact with Bet-ald in the OsBADH1 complex in which the interaction energies of W163 and N164 were higher than those in the other complexes (Fig. 4A). Additionally, interactions with Q294 and F397 were also important for OsBADH1–Bet-ald interactions. However, in OsBADH1–GAB-ald, E262, L263, C296 and W461 are the main residues for the attractive interaction with GAB-ald. Remarkably, N164, one of the catalytic triad residues, is also important for OsBADH1–GAB-ald (−1.17 kcal/mol); this was not observed from docking experiments. In the case of OsBADH2–Bet-ald, decomposition energies showed that six residues had strong attractive interactions with Bet-ald including Y163, M167, W170, E260, S295 and C453 (Fig. 4B).

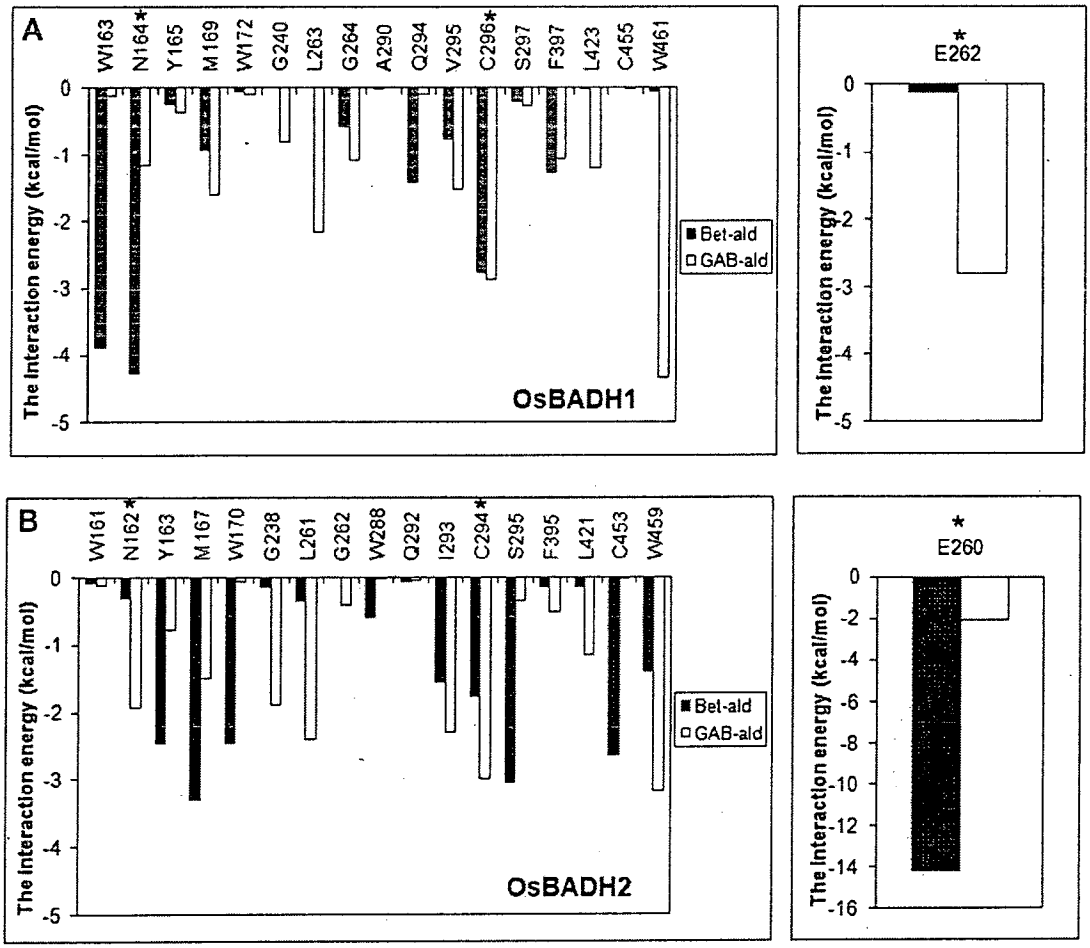

Fig. 4. Decomposition of binding free energies between aldehyde ligand and amino acid residues within 5 Å radius of this ligand within the OsBADH complexes (A) OsBADH1 (B) OsBADH2. The asterisk represents the catalytic triad residues.

It is noteworthy that E260 becomes the main residue having strong interactions with Bet-ald in this complex, suggesting that the negatively charge side chain of E260 interacts with the positive charge of the quaternary ammonium of Bet-ald. For OsBADH2–GAB-ald, four residues interact with GAB-ald including E260, L261, C294 and W459. This observation is in agreement with the result that four residues can form hydrogen bonds in the structure and that N162 is important for OsBADH2–GAB-ald (−1.93 kcal/mol). Taken together, the data from Fig. 4 indicates that interactions involving both OsBADH1–GAB-ald and OsBADH2–GAB-ald complexes are relatively similar. GAB-ald usually interacts with amino acid residues, N164, M169, E262, L263, V295, C296 and W461 in OsBADH1 and N162, M167, E260, L261, I293, C294 and W459 in OsBADH2, with the same position of the amino acid but a different spatial arrangement of GAB-ald. In contrast with GAB-ald, the interaction of Bet-ald in the complex is varied and a different spatial arrangement of Bet-ald was observed both in our MD simulations and in the crystal structure of BADH from *E. coli* [13]. This discrepancy may have stemmed from the fact that Bet-ald carries a positive charge and less hydrogen bonds are observed in the complex, leading to a large movement of the molecule, whereas GAB-ald can form several hydrogen bond networks to the enzyme thus generating a more rigid position within the substrate binding site.

According to our result, difference in amino acid residues between OsBADH1 (A290) and OsBADH2 (W288) may account for differences in substrate specificity between both OsBADHs. W288 of OsBADH2 can interact well with Bet-ald (−0.59 kcal/mol) but not GAB-ald. It has been proposed that W288 in PsAMADH2 affects the affinity of the enzyme without affecting the reaction rate [24]. However, this residue is also different between PsAMADH1 and PsAMADH2 (F288 for PsAMADH1 and W288 for PsAMADH2) [6]. The W288 side chain of PsAMADH2 reduces the volume of the substrate channel compared to F288 of PsAMADH1 [6]. Therefore, this residue may be key to the differences in substrate specificity observed among plant AMADH isoforms [24]. W288 of OsBADH2 reduces the volume of the substrate channel compared to A290 of OsBADH1. Bet-ald in the OsBADH2 complex can interact with W288 through π electron interactions between the positive charge of the quaternary ammonium and the negative charge of the W288 indole ring while in OsBADH1 this position is replaced by A290 which cannot form any interaction with Bet-ald [24]. Consistent with the results from PsAMADHs, W288 is the key residue in determining the substrate specificity in OsBADH isoforms in rice.

3.7. Conformation of the catalytic cysteine and glutamate

The conformation of catalytic Cys and Glu was observed from MD simulations of the OsBADH–ligand complexes. According to the previous study, the catalytic Cys residue can adopt two conformations: the "resting" conformation in which the Cys residue is far from the carbonyl carbon of the bound aldehyde [14].

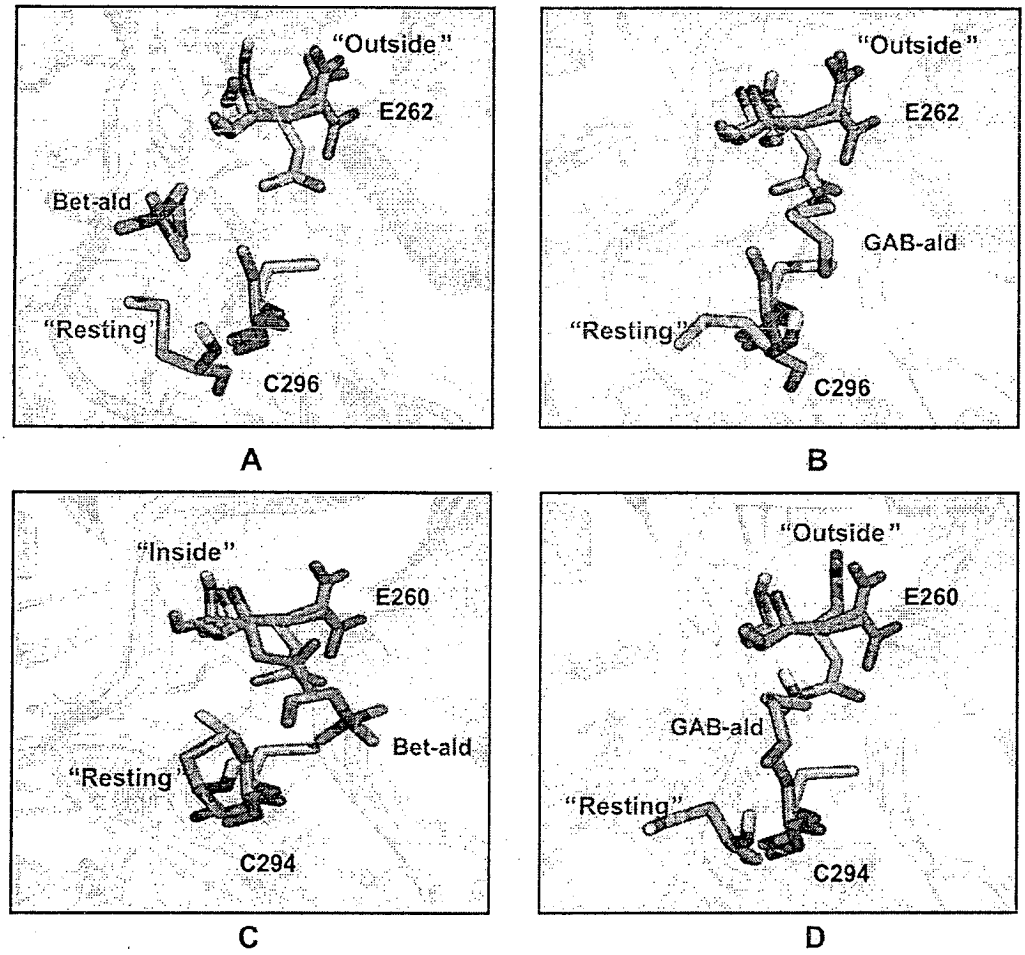

Fig. 5. The conformation of active site residues in OsBADH–substrate complexes from MD simulations compared to PaBADH (2WME) and ALDH2 (1O02). (A) OsBADH1 with Bet-ald (B) OsBADH1 with GAB-ald (C) OsBADH2 with Bet-ald (D) OsBADH2 with GAB-ald. The names of catalytic residues for OsBADH1 including C296, E262 while OsBADH2 including C294, E260 are shown in black text while the aldehyde substrates, Bet-ald and GAB-ald are shown in pink text. Side chain atoms of residue are shown in stick and colored by atoms (PaBADH carbon: salmon pink, ALDH2 carbon: lemon green, OsBADH1–Bet-ald carbon: green, OsBADH1–GAB-ald carbon: cyan, OsBADH2–Bet-ald carbon: orange, OsBADH2–GAB-ald carbon: magenta). (For interpretation of the references to color in this figure legend, the reader is referred to the web version of this article.)

and the "attacking" conformation in which the Cys residue is close to this carbon in the correct position to perform the nucleophilic attack [23]. In the case of the catalytic Glu residue, three possible conformations have been observed: the "inside" conformation in which the Glu residue can activate the catalytic Cys residue for nucleophilic attack, since its carboxyl group is close to the thiol [13,23], the "intermediate" conformation in which the Glu residue is suited for the activation of the hydrolytic water molecule [1,14,23], and the "outside" conformation in which the catalytic Glu releases the proton that was previously taken from either the catalytic Cys or a hydrolytic water involved in the proton relay mechanism [14,23].

The conformations of both catalytic residues from PaBADH (PDB codes 2WME) [14] and ALDH2 (PDB codes 1O02) [23] are shown in Supplementary data Fig. S5. When the structure of PaBADH is compared with the structure of ALDH2 and with OsBADH complexes from MD simulations (Fig. 5), it is revealed that the catalytic Glu residue in all structures exists in the "outside" conformation whereas the catalytic Cys residue is found in the "resting" conformation with the exception of the catalytic Glu residue of OsBADH2–Bet-ald complex that exists in an "inside" conformation. The negatively charged side chain of the catalytic Glu residue is positioned towards the positive quaternary ammonium of Bet-ald, suggesting it may have strong electrostatic interactions, consistent with the binding energy from MMGBSA decomposition. Additionally, the difference in the conformation of the catalytic Glu residue of OsBADH1 and OsBADH2 observed from MD simulations may also bring about the substrate specificity between the two substrates and the enzymes. Collectively, the work presented here for the first time provides the structure of OsBADH in complex with the substrates generated by MD simulations. Further studies on other residues in the substrate binding pocket to better understand the substrate specificity are in progress.

4. Conclusion

In this study, we describe the kinetic analysis of OsBADH1 and OsBADH2 wild-type and mutant enzymes using Bet-ald and GAB-ald as substrates. Kinetic results indicated that these enzymes would prefer GAB-ald to Bet-ald, which is in agreement with previous studies [9,10,17]. Out of the six mutants (N164A, W172A, W172F for OsBADH1 and N162A, W170A, W170F for OsBADH2), only the W172F of OsBADH1 and W170F of OsBADH2 mutants showed a higher catalytic efficiency towards GAB-ald, indicating that this position may be important for substrate specificity

towards GAB-ald. MD simulations suggested that GAB-ald forms hydrogen bonds with C296, E262, L263, and W461 in OsBADH1 and C294, E260, L261, and W459 in OsBADH2 better than Bet-ald. Decomposition energies revealed that W163, N164, Q294, C296 and F397 mainly interacted with Bet-ald in the OsBADH1–Bet-ald complex while E262, L263, C296 and W461 mainly interacted with GAB-ald in the OsBADH1–GAB-ald complex. In the OsBADH2–Bet-ald complex, Y163, M167, W170, E260, S295 and C453 displayed strong interactions and the strongest was with E260, suggesting that the negatively charged side chain of E260 interacts with the positively charged group of Bet-ald. E260, L261, C294 and W459 were shown to interact with GAB-ald in the OsBADH2–GAB-ald complex, which is consistent with the hydrogen bonding analysis. Our data indicate that the interactions of Bet-ald in the complex are varied in comparison with GAB-ald. This may be accounted for by a positive charge in Bet-ald and less hydrogen bond formation, leading to movement at various positions which can be observed in the MD simulation and the crystal structure of *E. coli* BADH [13]. In contrast, GAB-ald can form several hydrogen bonds, leading to a fixed position in the substrate binding site. One interesting point for the substrate recognition of OsBADHs is the difference in the amino acid residues at position 290 of OsBADH1 (A290) and position 288 of OsBADH2 (W288). W288 in OsBADH1 interacts with Bet-ald through π electron interactions but not with GAB-ald while A290 in OsBADH1 cannot form any interaction with the substrates. In plant PsAMADHs, the amino acid residue at position 288 has been proposed to play a key role in the difference in substrate specificity between both PsAMADHs isoforms (F288 for PsAMADH1 and W288 for PsAMADH2) [6]. Therefore, W288 is also a key residue in recognition and substrate specificity in OsBADH isoforms. We also compared the conformation of the catalytic residues, Cys and Glu with that of PaBADH and ALDH2. Results revealed that the catalytic Cys residue existed in the "resting" conformation in all structures whereas the catalytic Glu residue existed in the "outside" conformation except for Glu in OsBADH2–Bet-ald, which was found to adopt an "inside" conformation. It is suggested that the negatively charged side chain of catalytic Glu has strong electrostatic interactions with the positive quaternary ammonium of Bet-ald. This difference in the conformation of catalytic Glu residue of OsBADH1 and OsBADH2 may account for differences in substrate specificity between the two enzymes.

Acknowledgments

We thank National Nanotechnology Center (NANOTEC) for generously providing the discovery studio software and the National Electronics and Computer Technology Center (NECTEC) for providing computational resources. This research was supported by Kasetsart University Research and Development Institute (grant: v-t(d)43.54), Faculty of Science (grant: ScRF-S10/2553), Graduate School Kasetsart University and Thailand Research Fund (grant: RTA5380010). Financial support from the Center of Excellence for Innovation in Chemistry (PERCH-CIC), Commission on Higher Education, Ministry of Education is also gratefully acknowledged.

Appendix A. Supplementary material

Supplementary material associated with this article can be found, in the online version, at doi:10.1016/j.biochi.2012.04.009.

References

[1] Z.J. Liu, Y.J. Sun, J. Rose, Y.J. Chung, C.D. Hsiao, W.R. Chang, I. Kuo, J. Perozich, R. Lindahl, J. Hempel, B.C. Wang, The first structure of an aldehyde dehydrogenase reveals novel interactions between NAD and the Rossmann fold, Nat. Struct. Biol. 4 (1997) 317–326.
[2] A. Yoshida, A. Rzhetsky, L.C. Hsu, C. Chang, Human aldehyde dehydrogenase gene family, Eur. J. Biochem. 251 (1998) 549–557.
[3] J. Perozich, H. Nicholas, B.-C. Wang, R. Lindahl, J. Hempel, Relationships within the aldehyde dehydrogeanse extended family, Protein Sci. 8 (1999) 137–146.
[4] P.N. Moschou, K.A. Paschalidis, K.A. Roubelakis-Angelakis, Plant polyamine catabolism: the state of the art, Plant Signal. Behav. 3 (2008) 1061–1066.
[5] M. Šebela, F. Brauner, A. Radová, S. Jacobsen, J. Havliš, P. Galuszka, P. Pe&ccaron, Characterisation of a homogeneous plant aminoaldehyde dehydrogenase, Biochim. Biophys. Acta 1480 (2000) 329–341.
[6] M. Tylichová, D. Kopecný, S. Moréra, P. Briozzo, R. Lenobel, J. Snégaroff, M. Šebela, Structural and functional characterization of plant aminoaldehyde dehydrogenase from *Pisum sativum* with a broad specificity for natural and synthetic aminoaldehydes, J. Mol. Biol. 396 (2010) 870–882.
[7] T.L. Fitzgerald, D.L.E. Waters, R.J. Henry, Betaine aldehyde dehydrogenase in plants, Plant Biol. 11 (2009) 119–130.
[8] T. Fujiwara, K. Hori, K. Ozaki, Y. Yokota, S. Mitsuya, T. Ichiyanagi, T. Hattori, T. Takabe, Enzymatic characterization of peroxisomal and cytosolic betaine aldehyde dehydrogenases in barley, Physiol. Plant 134 (2008) 22–30.
[9] L. Bradbury, S. Gillies, D. Brushett, D. Waters, R. Henry, Inactivation of an aminoaldehyde dehydrogenase is responsible for fragrance in rice, Plant Mol. Biol. 68 (2008) 439–449.
[10] S. Mitsuya, Y. Yokota, T. Fujiwara, N. Mori, T. Takabe, OsBADH1 is possibly involved in acetaldehyde oxidation in rice plant peroxisomes, FEBS Lett. 583 (2009) 3625–3629.
[11] P. Weigel, E.A. Weretilnyk, A.D. Hanson, Betaine aldehyde oxidation by spinach chloroplasts, Plant Physiol. 82 (1986) 753–759.
[12] K. Johansson, M. El-Ahmad, S. Ramaswamy, L. Hjelmqvist, H. Jornvall, H. Eklund, Structure of betaine aldehyde dehydrogenase at 2.1 A resolution, Protein Sci. 7 (1998) 2106–2117.
[13] A. Gruez, V. Roig-Zamboni, S. Grisel, A. Salomoni, C. Valencia, V. Campanacci, M. Tegoni, C. Cambillau, Crystal structure and kinetics identify *Escherichia coli* YdcW gene product as a medium-chain aldehyde dehydrogenase, J. Mol. Biol. 343 (2004) 29–41.
[14] L. González-Segura, E. Rudiño-Piñera, R.A. Muñoz-Clares, E. Horjales, The crystal structure of a ternary complex of betaine aldehyde dehydrogenase from *Pseudomonas aeruginosa* provides new insight into the reaction mechanism and shows a novel binding mode of the 2'-phosphate of $NADP^+$ and a novel cation binding site, J. Mol. Biol. 385 (2009) 542–557.
[15] L.M.T. Bradbury, T.L. Fitzgerald, R.J. Henry, Q. Jin, D.L.E. Waters, The gene for fragrance in rice, Plant Biotechnol. J. 3 (2005) 363–370.
[16] S. Chen, Y. Yang, W. Shi, Q. Ji, F. He, Z. Zhang, Z. Cheng, X. Liu, M. Xu, Badh2, encoding betaine aldehyde dehydrogenase, inhibits the biosynthesis of 2-acetyl-1-pyrroline, a major component in rice fragrance, Plant Cell 20 (2008) 1850–1861.
[17] R. Wongpanya, N. Boonyalai, N. Thammachuchourat, N. Horata, S. Arikit, K. Myint, A. Vanavichit, K. Choowongkomon, Biochemical and enzymatic study of rice BADH wild-type and mutants: an insight into fragrance in rice, Protein J. 30 (2011) 529–538.
[18] B. Kuaprasert, K. Silprasit, N. Horata, P. Khunrae, R. Wongpanya, N. Boonyalai, A. Vanavichit, K. Choowongkomon, Purification, crystallization and preliminary X-ray analysis of recombinant betaine aldehyde dehydrogenase 2 (OsBADH2), a protein involved in jasmine aroma, from Thai fragrant rice (*Oryza sativa* L.), Acta Crystallog. Sect. F 67 (2011) 1221–1223.
[19] W.L. Delano, The PyMOL molecular graphics system, DeLano Scientific (2002).
[20] G.M. Morris, D.S. Goodsell, R.S. Halliday, R. Huey, W.E. Hart, R.K. Belew, A.J. Olson, Automated docking using a Lamarckian genetic algorithm and an empirical binding free energy function, J. Comput. Chem. 19 (1998) 1639–1662.
[21] W. Cornell, P. Cieplak, C. Bayly, I. Gould, K. Merz, D. Ferguson, D. Spellmeyer, T. Fox, J. Caldwell, P. Kollman, A second generation force field for the simulation of proteins, nucleic acids, and organic molecules, J. Am. Chem. Soc. 117 (1995) 5179–5197.
[22] W.L. Jorgensen, J. Chandrasekhar, J.D. Madura, R.W. Impey, M.L. Klein, Comparison of simple potential functions for simulating liquid water, J. Chem. Phys. 79 (1983) 926–935.
[23] S.J. Perez-Miller, T.D. Hurley, Coenzyme isomerization is integral to catalysis in aldehyde dehydrogenase, Biochemistry 42 (2003) 7100–7109.
[24] D. Kopečný, M. Tylichová, J. Snegaroff, H. Popelková, M. Šebela, Carboxylate and aromatic active-site residues are determinants of high-affinity binding of ω-aminoaldehydes to plant aminoaldehyde dehydrogenases, FEBS J. 278 (2011) 3130–3139.
[25] R.A. Laskowski, M.W. MacArthur, D.S. Moss, J.M. Thornton, PROCHECK: a program to check the stereochemical quality of protein structures, J. Appl. Crystallogr. 26 (1993) 283–291.